Measures of intermittency in driven supersonic flows

D. Porter,[1] A. Pouquet,[2] and P. Woodward[1]
[1]*Department of Astronomy, University of Minnesota, 116 Church Street SE, Minneapolis, Minnesota 55455*
[2]*NCAR, P.O. Box 3000, Boulder, Colorado 80307*
and CNRS, UMR 6529, Observatoire de la Côte d'Azur, Boîte Postale 4229 06304 Nice Cedex 4, France
(Received 7 March 2002; published 12 August 2002)

Scaling exponents for structure functions of the velocity, density, and entropy are computed for driven supersonic flows for rms Mach numbers of order unity, with numerical simulations using the piecewise parabolic method algorithm on grids of up to 512^3 points. The driving is made up of either one or three orthogonal shear waves. In all cases studied, the compressible component of the velocity in the statistically steady regime is weaker than its solenoidal counterpart by roughly a factor of 6. Exponents for the longitudinal component of the velocity are comparable to what is found in the incompressible case and appear insensitive to the presence of numerous shocks. Scaling exponents of the transverse components of the velocity are comparable to those for the longitudinal component. Density and entropy structure functions display strong departures from linear scaling. Finally, the scaling of structure functions of the energy transfer is also given and compared with the Kolmogorov refined similarity hypothesis.

DOI: 10.1103/PhysRevE.66.026301 PACS number(s): 47.27.Gs, 47.40.−x, 47.27.Jv

I. INTRODUCTION

Turbulent flows are pervasive, being observed in many geophysical and astrophysical situations, in particular when one has access to a wide range of scales as in the planetary boundary layers, or from radio scintillations in the interstellar medium, as well as in the solar environment both at the level of the photosphere and of the corona, or in the solar wind. One of the characteristic features of such flows is their intermittency, i.e., the scarcity both in time and in space of strong structures as diagnosed, for example, by histograms—of velocity derivatives or of the density field—with non-Gaussian wings. These strong wings may be linked with the presence of a hierarchy of intense small-scale structures such as shocks and vortex filaments, as well as voids as observed in [1] for decaying supersonic flows.

A quantitative measurement of such an intermittent behavior is obtained from the determination of anomalous scaling exponents of structure functions of the physical fields. Specifying the definitions to the velocity, one writes the velocity difference over a distance r assuming homogeneity, as

$$\delta\mathbf{u}(\mathbf{r}) = \mathbf{u}(\mathbf{x}+\mathbf{r}) - \mathbf{u}(\mathbf{x});$$

its longitudinal (respectively transverse) components are

$$\delta\mathbf{u}_L(\mathbf{r}) = [\,\delta\mathbf{u}(\mathbf{r})\cdot\hat{\mathbf{r}}]\hat{\mathbf{r}}$$

[respectively $\delta\mathbf{u}_T(\mathbf{r}) = \delta\mathbf{u}(\mathbf{r}) - \delta\mathbf{u}_L(\mathbf{r})$], where $\hat{\mathbf{r}}$ is the unit vector along the separation $\mathbf{r}$. The longitudinal (respectively transverse) structure functions of order p read, assuming also isotropy so that both transverse components in three dimensions can be assimilated to one field of common rms amplitude v_T:

$$S_{p;L}(\mathbf{r}) = \langle\,\delta\mathbf{u}_L^p(\mathbf{r})\rangle \sim r^{\zeta_p^L} \tag{1}$$

and

$$S_{p;T}(\mathbf{r}) = \langle\,\delta\mathbf{u}_T^p(\mathbf{r})\rangle \sim r^{\zeta_p^T}, \tag{2}$$

where it is assumed that there exists a range within which self-similarity applies and such structure functions follow power laws. As the order p of these functions increases, they become dominated by the most intense structures i.e., they indeed convey a signature of intermittency.

Whereas an extension to all orders of the Kolmogorov law (or K41) [2] for the energy spectrum in the incompressible case predicts a linear variation for the scaling exponents of $S_{p;L}$ with a slope of 1/3 (see, e.g., [3] for a recent account), both experimental and numerical data indicate a clear departure from this law. Numerous phenomenological models attempt to reproduce these exponents; amongst those, the She-Leveque model [4] (or SL model), which can be viewed as parameter-free (see, however, [5,6]), stands out because of its excellent agreement with data; the log-normal model, with the choice of its open parameter $\mu = 0.21$, agrees as well with the data.

On the other hand, several recent experimental and numerical investigations [7] disagree among themselves as to what such exponents might be for the transverse components of the velocity, with up to now no clear distinction of which component, longitudinal or transverse, if any, is more intermittent, i.e., with stronger departures from the K41 linear law $\zeta_p = p/3$. Whether such discrepancies between the measured ζ_p^L and ζ_p^T exponents are in fact attributable to poor statistics linked with insufficiently large data sets, or whether they are intrinsic—reflecting a lack of universality among flows—is not entirely clear yet. However, there is now evidence pointing to a Reynolds number dependence [8] with the two sets of exponents becoming equal at high Reynolds number, thus recovering full isotropy, at least for an isotropic forcing (see [9] for a review centered on the study of the passive scalar).

The present work aims at testing the domain of universality of such laws by investigating the case of supersonic

flows. Several observational data sets indicate that the exponents of velocity structure functions vary in a nonlinear fashion with their order, as for the solar wind [10] and the interstellar medium (see [11] for a review). Such astrogeophysical flows are both compressible and turbulent, and in both cases magnetic fields play a dynamic role as well. However, as a first investigation, one can restrict the analysis to the case of neutral fluids in order to concentrate on the nature of the modifications that may be brought forth by compressibility alone [12].

After describing the methodology in the next section, we give the results concerning the intermittent properties of the velocity in Sec. III and of the energy transfer in Sec. IV; the last section is the Conclusion.

II. METHODOLOGY

A. The equations

The approach we take is numerical, using the piecewise parabolic method (or PPM) first introduced in [13]; it implements an algorithm that guarantees little dissipation in the large scales, with shocks together with sharp gradients for all variables concentrated on a few grid points at small scales. The PPM algorithm has been tested against the Navier-Stokes equations for decaying flows both in two dimensions [14] and recently in three dimensions [15] (see also [16,17]) up to resolutions of 1024^2 and 512^3 grid points, respectively. The agreement obtains at all scales, with, however, a lesser dissipation for the PPM flow on a given grid resulting in a more developed energy spectrum.

The equations for the density ρ, the velocity $\mathbf{u}$, the pressure P, and the internal energy e are now given for reference, with $\mathbf{F}$ a mechanical forcing term corresponding to an acceleration, and Λ a cooling function:

$$\frac{\partial \rho}{\partial t} + \nabla \cdot (\rho \mathbf{u}) = 0, \tag{3}$$

$$\frac{\partial \mathbf{u}}{\partial t} + \mathbf{u} \cdot \nabla \mathbf{u} = -\frac{\nabla P}{\rho} + \mathbf{F}, \tag{4}$$

$$\frac{\partial e}{\partial t} + \mathbf{u} \cdot \nabla e = -(\gamma - 1) e \nabla \cdot \mathbf{u} - \Lambda, \tag{5}$$

$$P = (\gamma - 1) \rho e. \tag{6}$$

Note that this formulation of an acceleration in the velocity equation (as opposed to a force in the momentum equation) avoids small-scale driving because of small-scale density variations.

In order to obtain an equilibrium system, i.e., to maintain a constant (on average) Mach number, we compensate for the heating occurring both in shocks and because of the energy input $\langle \mathbf{u} \cdot \mathbf{F} \rangle$ in the driven runs by a temperature-dependent cooling function Λ reminiscent of Stefan's law applicable to optically thick media; this cooling function thus reads:

$$\Lambda = \sigma T^4$$

with $\sigma = 0.098\,344\,8$ for both runs 1 and 3.

Three computations are analyzed, all with periodic boundary conditions. Run 3 corresponds to a flow driven by three shear waves in three orthogonal directions, and at the largest wave number allowed by the computation, viz. $F_i = A_p \sin(2\pi x_j / L_0) \hat{e}_k$ with the triplet (i,j,k) a cyclic permutation of the coordinates (X,Y,Z), and where $L_0 = 2\pi$ is the length of the computational box. In run 1, only one component of the previous force is kept, i.e., the driving is a one-dimensional shear wave; computations for run 1 were also mentioned briefly in [16]. We take $A_p = 1$ for run 1 and $A_p = 4$ for run 3. Both runs are computed on a grid of 512^3 points. For run 1, $\gamma = 1.4$ and $\gamma = 5/3$ for run 3.

At $t = 0$, the flow has uniform density with $\rho_0 = 1$ and uniform pressure; it is embedded in a random velocity field with a prescribed spectrum $E(k) \sim k^4 \exp(-k^2)$ as in [14–18]. It is then left to settle on a low resolution grid of 128^3 points for more than 100 turnover times τ_{NL} (with $\tau_{NL} = \tau_{ac}$ where τ_{ac} is the acoustic time); the grid is then upgraded to 256^3, and the flow is again left to settle for $14\tau_{NL}$; this procedure is iterated up to the final resolution of 512^3 points on which the computation is first run for $2\tau_{NL}$ before the statistical analysis is started. For run 3, 14 temporal states are then retained, separated by $0.2\tau_{NL}$, leading to a data set of $\sim 1.9 \times 10^9$ points. A temporal subsampling with a refinement factor of 20 has been stored as well in order to study the short-time variations of the intermittency exponents over a total time span of $2\tau_{NL}$. A similar analysis is implemented for run 1.

We show in Fig. 1 the resulting temporal evolution for run 3 of the total kinetic energy E_k (top) and the total internal energy E_i (bottom), where the time is in units of the acoustic time. A statistically steady state with exchanges between the two forms of energy takes place at the 10% level, with a phase lag between E_k and E_i. The total energy (not shown) varies with time as well because of the forcing and the cooling.

B. The degree of compressibility of the flow

The resulting flow consists of a superposition of planar shocks, slip surfaces, and vortex filaments with a lifetime of a few eddy turnover times, similar to the case of the temporal evolution of the decay problem [1]. Such flows are characterized by fully developed Fourier spectra with approximate $-5/3$ slopes for both the solenoidal component $\mathbf{u}_V$ and the compressible component $\mathbf{u}_C$ of the velocity, and with on average a ratio of compressive to solenoidal modal energy

$$\chi = E_C / E_V \tag{7}$$

close to 3%, where one refers here to the Helmholtz decomposition of the velocity into a divergence-free (or solenoidal, i.e., vortex-like $\mathbf{u}_V$) component, and a curl-free (or compressive, i.e., shock-like $\mathbf{u}_C$) component of respective energy E_V and E_C, with $E_k = E_C + E_V$. For both runs, the rms Mach number is close to unity on average, and density fluctuations $\delta\rho/\rho$ are of the order of 25%; the rms velocity is $u_0 \sim 1.2$ and the integral scale is of the order of $l_0 \sim 0.5 L_0$ [18].

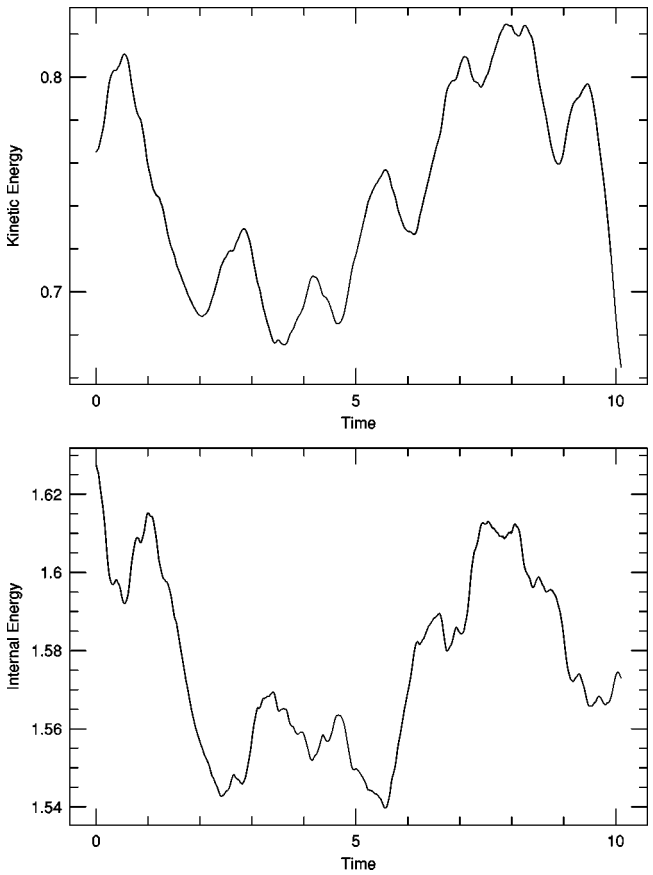

FIG. 1. Temporal evolution for run 3 of the kinetic energy (top) and internal energy (bottom). All quantities are nondimensional.

In all computations of decaying two-dimensional turbulence, the resulting value of the parameter χ defined above after a few eddy turnover times is always of the order of 10% or less (see, e.g., [19]). Computations in three dimensions on a grid of 256^3 points gives similar results. We show in Fig. 2 the temporal evolution for three such computations, with initially, respectively, $\chi=0.10$ (solid line) and $\chi=0.90$

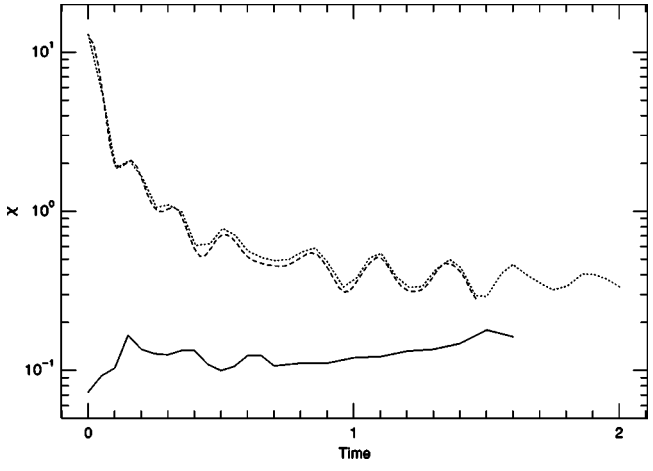

FIG. 2. Temporal evolution of $\chi=E^C/E^V$ [see Eq. (7)] for three-dimensional decay computations with initially $\chi=0.1$ (solid line) and $\chi=0.9$ (dash lines) at different resolutions.

(dash lines), and all other parameters identical (see [21]). In the latter case dominated by compressional modes initially, this ratio evolves rapidly to a moderate value because of the fast formation and dissipation of shocks; the two dashed curves correspond to two different resolutions for the same computation (namely grids of 64^3 and 128^3 points). After several eddy turnover times, these ratios for the three runs become comparable, and the flows are dominated by the vortical component of the velocity although there are still numerous shocks present in the fluid even at late times.

In the case of driven flows, such computations have a huge cost because of both the rather slow rate for reaching a statistically steady state, and also for the need of fair sampling over a sufficiently representative realization of the fluctuations over time. Under such circumstances, no systematic high-resolution three-dimensional parametric study has been performed. However, in the many cases that have been run, the parameter χ remains of the order of 10%, with one exception: it was shown in [22] that when the forcing is purely compressional (either an expansion wave in the momentum equation or heating terms in the energy equation, such as would result from the blast wave emanating from a supernova or from cosmic rays or ionization winds from O stars in the interstellar medium), and in the absence of both rotation and of magnetic fields, then the vorticity never gets very large and the parameter χ in the steady state settles to a value close to unity.

The compressibility of the flow is traditionally measured by the Mach number. We show in Fig. 3 a histogram of the Mach number for run 3. The mean is 0.97 with excursions up to $M_{max}=3.5$ and with 50% of the flow having a local Mach number of unity or above. Several other histograms are given in Fig. 3, namely the divergence of the velocity, the vorticity (absolute value), for which a clear exponential scaling obtains, and the density. Note that the histogram of divergence is asymmetric, with substantially stronger values for rarefaction waves, and that vorticity develops even stronger values. We also note that the density develops, for low values, power-law wings, with an exponent close to 4 (not shown).

One-dimensional cuts of the divergence and of the vorticity are given in Fig. 4 (respectively, top and bottom, see labels) at the same time and for the same run as for Fig. 3. These fields display strong fluctuations, with substantially higher values for the vorticity; this is linked to the shear-wave driving of the flow, with $\mathbf{u}_C/\mathbf{u}_S\sim 0.18$ in the steady state. The second-order longitudinal (crosses) and transverse (circles) structure functions of the velocity are given as well in Fig. 4; the solid line represents the Kolmogorov scaling; finally, the energy spectra for the solenoidal (dash line), compressible (dotted line), and total square velocity (solid line) are also shown. All three spectra are compensated by a K41 $\epsilon^{2/3}k^{-5/3}$ law, where ϵ is the time averaged energy transfer rate per unit mass. The second-order structure functions shown in Fig. 4 present a nearly linear behavior of more than a decade in scale. These structure functions were derived by taking displacements purely along the axes (XYZ method described below), which are aligned with the large scale driving force. This method of sampling is most sensitive to the large scale anisotropy due to the driving force.

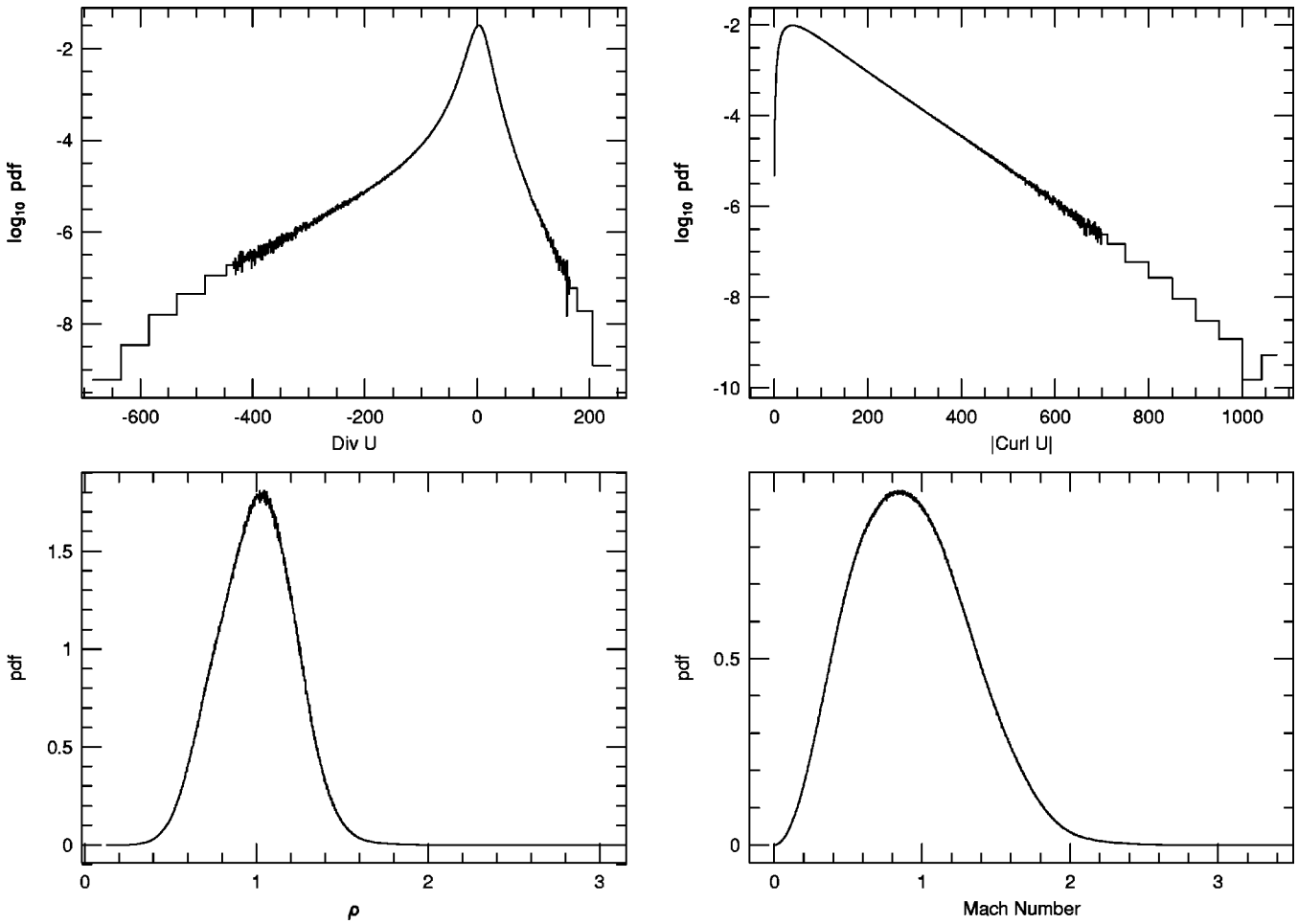

FIG. 3. Histograms for run 3 at $t=9.2$ of the divergence of the velocity, the vorticity magnitude, the density, and the Mach number (see labels). Logarithmic counts are performed on the vertical axis for the first two histograms. Note the clear exponential wings for both derivative fields constructed on the velocity.

The variation in the slope of $\langle|\delta U_T|^2\rangle$ seen in Fig. 4 can be associated with this anisotropy. When the structure functions are derived from data collected along displacements at many different angles relative to the large scale driving the scalings are much improved. This ''LT'' method, where LT stands for collecting the longitudinal and transverse components of velocity relative to arbitrarily oriented spatial displacements, is described below. For example, the transverse second-order structure functions of the velocity, collected via the LT method, when compensated by the She-Leveque scaling [4] $\delta X^{\zeta(2)}$ [see Fig. 8(b)] are constant to within 2.5% of their average value over a factor of 16 in displacement. Even with the structure functions shown in Fig. 4, which are derived from the XYZ method—most sensitive to imposed driving force anisotropies, the maximum variation of these compensated second-order structure functions is 7% over the same range of displacement.

By contrast, the compensated Fourier spectra—and particularly the solenoidal component—have two bumps which are much larger in amplitude. The one at large scale corresponds to the adjusting between the energy-containing range and the inertial range. The one at small scale, rather prominent with an overshooting—as compared to the Kolmogorov law—by more than a factor of 2, smears the scaling; it corresponds to a Gibbs-like effect due to the abrupt ending of the variation of the structure function in configuration space at the onset of the dissipative range; it can also be modeled by the so-called bottleneck effect for incompressible flows, whereby the energy cascading to small scales encounters abruptly the dissipation range with significantly less energy. The compensated energy spectra $k^{5/3}E(k)/\epsilon^{2/3}$ plotted in Fig. 4 are essentially a measure of the Kolmogorov constant, C_K, for this Mach one driven flow. We find that C_K is within 45% of 1.5 for KL_0 in the range from 7 to 549, where L_0 is the size of the box so that $k_{min}L_0=2\pi$ and $k_{max}L_0=512\pi$. Experimental evaluations of C_K for incompressible flow give a value close to 1.5 as well. The similarity in C_K between incompressible flows and this compressible one may be due to the dominance of the solenoidal modes, which is a result of the pure solenoidal driving.

Finally, we note that in the statistically stationary regime, the Taylor wave number saturates at a value close to 16.8 and the integral wave number is close to 1.9. The resulting effec-

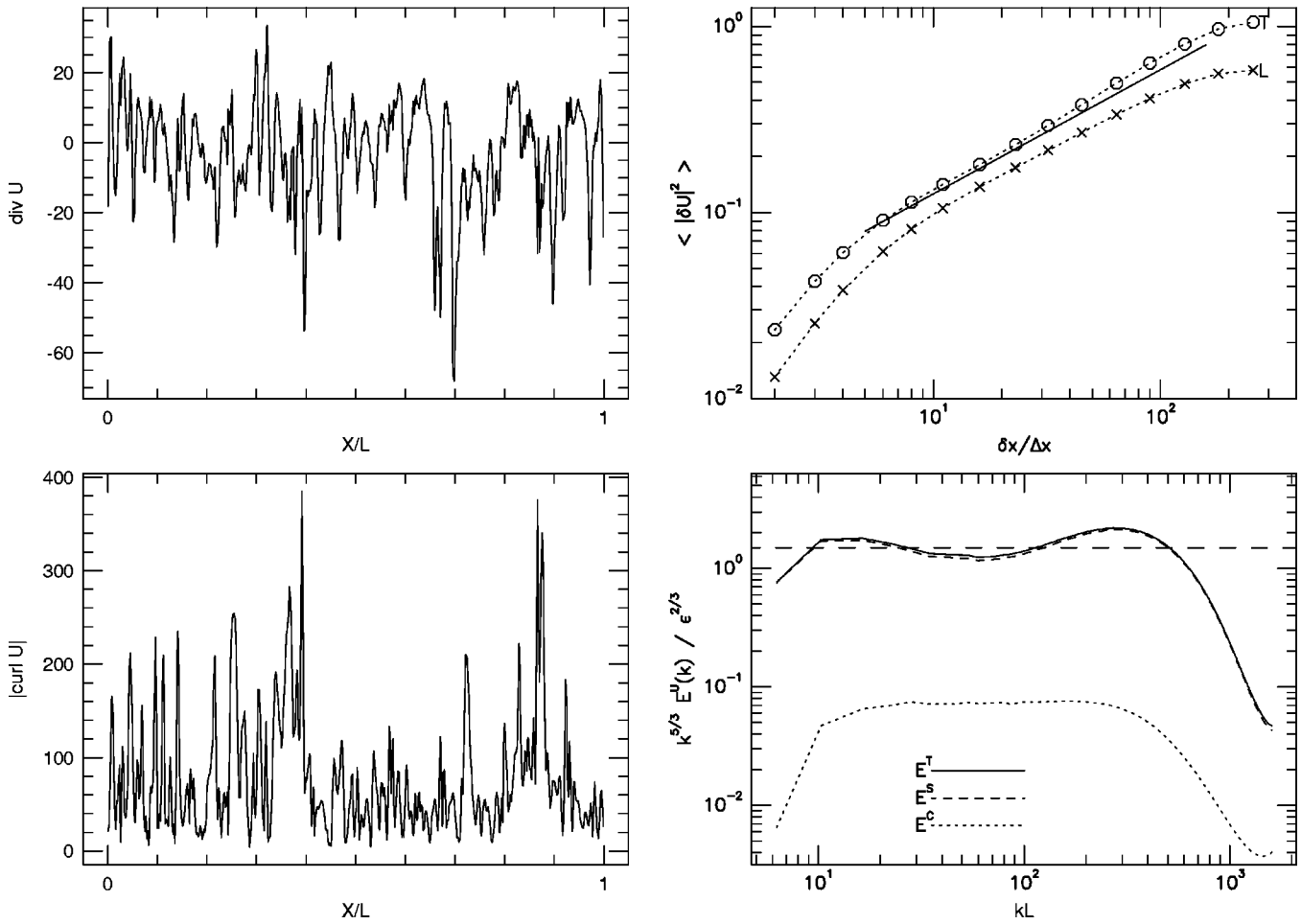

FIG. 4. One-dimensional cut through the computational box of the divergence of the velocity (top) and the vorticity (bottom); second-order longitudinal (crosses) and transverse (circles) structure functions of the velocity; the solid line represents the K41 law; and finally the energy spectra for the solenoidal (dashed line), compressible (dotted line), and total square velocity (solid line)—all three spectra compensated by a K41 $\epsilon^{2/3}k^{-5/3}$ law, which ϵ is the energy transfer rate per unit mass. A value of $C_K=1.5$ is indicated by the horizontal long-dashed line. All figures are given for run 3a at the same time as for Figs. 1 and 3.

tive Taylor-based Reynolds number (see, e.g., [1]) is thus of the order of 80, with moreover negligible dissipation in the large scales, because of the numerical algorithm used here.

C. The structures of the flow

Figure 5 shows (top left) the entropy and (top right) the vorticity, together with (bottom left) the divergence of the velocity and finally (bottom right) the energy transfer; all of these grayscale images are given for run 3 at time 9.2 in a section of the volume which spans the whole X and Y extent of the simulation, and Z in the interval $[0.6,0.7]L_0$.

Note the significant spatial correlation—both at strong values and for voids—between all variables which can be seen as representing different stages of evolution of the flow. All fields are mostly of a filamentary nature, at least at high values. These images are thresholded in amplitude at from about 1 to about 8 σ: the entropy, the vorticity, the divergence of velocity, and the forward transfer are thresholded respectively at 0.83 σ above the mean, 2 σ above zero, 2.6 σ below zero (thus showing only compression), and 7.54 above the mean (thus showing only very strong forward transfer). Less extreme variations, in each case, are rendered transparent. Furthermore, note that the hot spots in the energy transfer are mostly associated with strong vortex filaments. What is perhaps more striking is that such filaments, from interactions such as intertwining, organize on larger scales as larger filaments, the latter being clearly delineated in the other three variables displayed here. The strong sheet-like structures in the divergence of the velocity are also producing significant energy transfer. The density also organizes in patches with regions delineating either the vorticity filaments or the shocks.

At intermediate amplitudes, a wealth of structures emerge (not shown): for example, besides filaments, both sheets and spirals are found as well in the vorticity [16].

III. INTERMITTENCY OF COMPRESSIBLE FLOWS

Numerous studies have shown that strongly localized structures in vorticity, divergence, and entropy as well as for the energy transfer develop through dynamical interactions. We now proceed in assessing in a quantitative way the intermittency of supersonic flows through the determination of

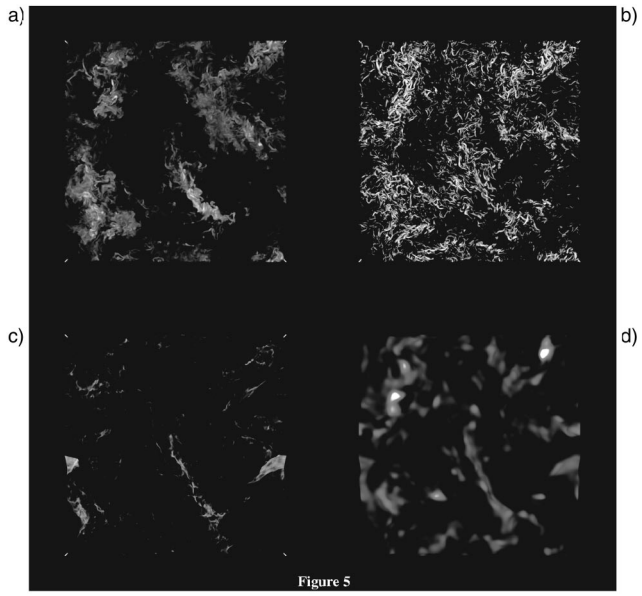

FIG. 5. Grayscale images for run 3 at time 9.2 of (a) (top left): the entropy; (b) (top right): the vorticity; (c) (bottom left): the divergence of the velocity; and finally (d) (bottom right): the energy transfer. In each case the ramp in grayscale is linear and ramps from black to white, respectively, over the ranges [0.83,8.76] σ over the average for entropy, [2,4] σ above zero for vorticity, [2.6,21.2] σ below zero for divergence of velocity (showing only compression), and [7.54,78.32] σ above the mean for transfer, showing only strong forward transfer. Note the similar filamentary structures in all fields.

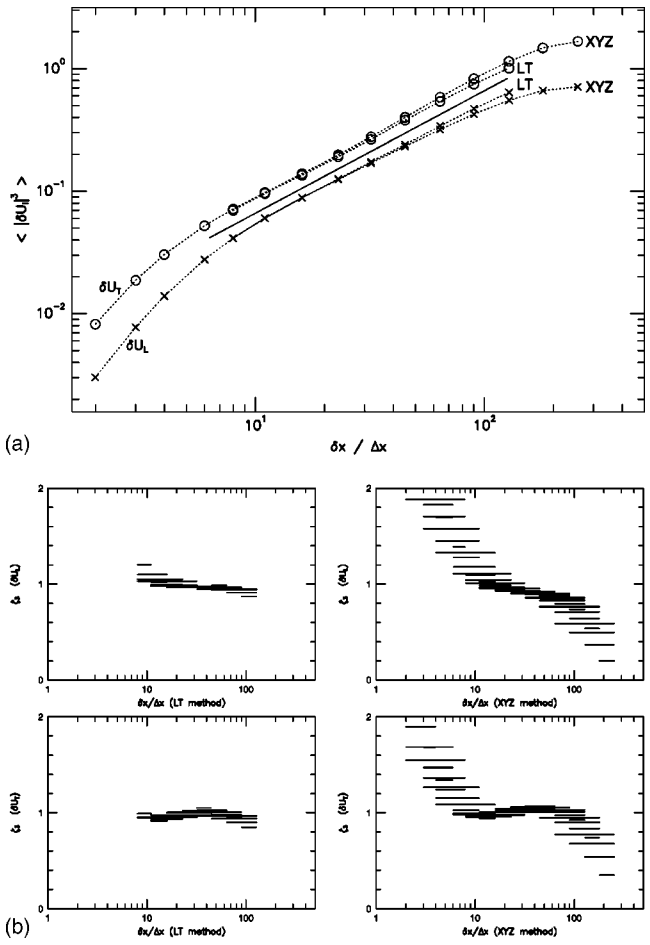

FIG. 6. (a) Third-order velocity structure functions for run 3 averaged over 24 snapshots evenly spaced from time 2 to 4.6, for u_L (circle) and u_T (cross) and using either the XYZ or the LT method, as labeled. Log-log coordinates are used. (b) Local slopes for the same structure functions with u_L on the top and u_T on the bottom, with the LT method on the left and the XYZ method on the right.

scaling laws of structure functions of order higher than that for the energy, and for various physical fields, beginning with the velocity.

A. The longitudinal and transverse components of the velocity

Structure functions are constructed for the longitudinal and transverse components of the velocity field, and for the density and entropy as well, with, respectively, $S_{p;L}(\mathbf{r}) \sim r^{\zeta_p^L}$ for the longitudinal component of the velocity, $S_{p;T}(\mathbf{r}) \sim r^{\zeta_p^T}$ for its transverse component, $S_{p;\rho}(\mathbf{r}) \sim r^{\zeta_p^\rho}$ for the density, and $S_{p;\mathcal{S}}(\mathbf{r}) \sim r^{\zeta_p^\mathcal{S}}$ for the entropy. For the polytropic ideal gas considered here, the density and pressure field varaibles may be scaled by a constant numerical factor: the same flow evolution will result, with only an appropriate scaling of time. Thus, in terms of the evolution of the flow and of the structures, density contrasts—as opposed to density differences—is what matters. Typical density contrasts are of order unity in the flows presented here, a statistical measure of density fluctuations which is not skewed by positive definiteness is desired. Hence, in characterizing variations in density it is most appropriate to construct structure functions based on the differences in the logarithm of the density, viz. $S_{p;\rho}(\mathbf{r}) = \langle \delta l_\rho^p(\mathbf{r}) \rangle$ where $l_\rho = \log \rho$.

Absolute values of velocity differences are employed, in order to improve the signal-to-noise ratio. The intermittency exponents ζ_p^α (with $\alpha = L,T,\rho,S$) are computed in two different fashions. On the one hand, displacement vectors $\mathbf{r}$ are taken along the grid axes, i.e., in the XYZ directions. But since the forcing for run 3 is along XYZ as well, a second method (named LT) was implemented whereby the displacements are taken in all individual (say, horizontal) planes with averaging over a set of up to 12 angles in each plane, depending on the value of the modulus of $\mathbf{r}$. This method allows for a more isotropic evaluation of the exponents (see [20] for a discussion of isotropy in the context of intermittency), although full isotropy would only be recovered by using the data in the third direction as well, a task left for future work. As stated before, the data is built with 14 temporal snapshots separated by 0.2 eddy turnover times, with a total of 1.5×10^9 data points.

The extent of the inertial range over which the slopes of structure functions are computed is obtained by examination of both $S_{3;L}$ and $S_{8;L}$. Their scaling for run 3 (using absolute values of velocity differences) are displayed in Figs. 6(a) and 7(a) for both u_L (circle) and u_T (cross) and using both the LT and XYZ methods (see labels on curve). For the LT method,

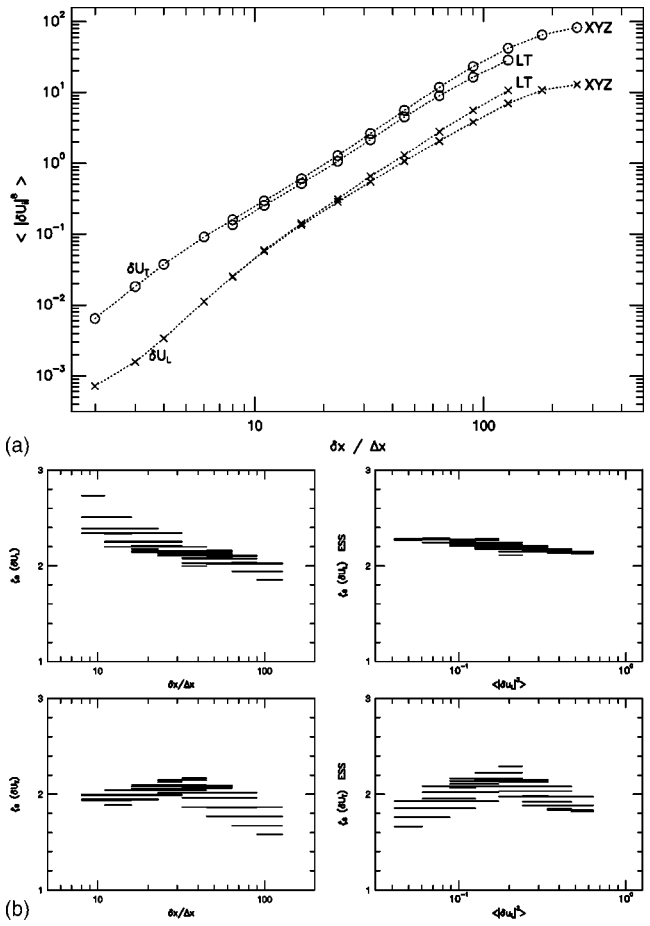

FIG. 7. (a) Eighth-order velocity structure functions for run 3 averaged over 24 snapshots evenly spaced from time 2 to 4.6, for u_L (circle) and u_T (cross) and using either the XYZ or the LT method, as labeled. Log-log coordinates are used. (b) Local slopes for the same structure functions with u_L on the top and u_T on the bottom, using the ESS methodology on the right and direct slopes on the left. All four sets are measured using the LT method. There is significantly less scatter in the slopes using the ESS methodology, especially for u_L.

the range within which scaling applies [11,64] is in units of the grid spacing $\delta x = 2\pi/512$. We checked that both methods give the same exponents to within a few percent when the interval is reduced to $[11\delta x, 23\delta x]$; larger errors (of the order of 10%) arise in the XYZ method, and the discrepancy between the two methods increases with increasing order of the structure function, but is negligible at the order examined here. Indeed, the data in Fig. 7(a) for $p=8$ shows a lesser range of linear scaling.

A study of the local (as opposed to global) slopes of these curves confirms this diagnostic (see also [18]) as shown in Fig. 6(b) for $p=3$ and Fig. 7(b) for $p=8$. In Fig. 6(b) we give these local slopes with $\mathbf{u}_L$ (top two) and $\mathbf{u}_T$ (bottom two), using the LT method (left) or the XYZ method (right). In Fig. 7(b) slopes calculated from moments collected via the LT method are shown and contrasted with results from the so-called extended self-similar (or ESS) methodology [23] (see discussion below). In both Figs. 6(b) and 7(b), the extent of each line indicates the domain over which the local slope

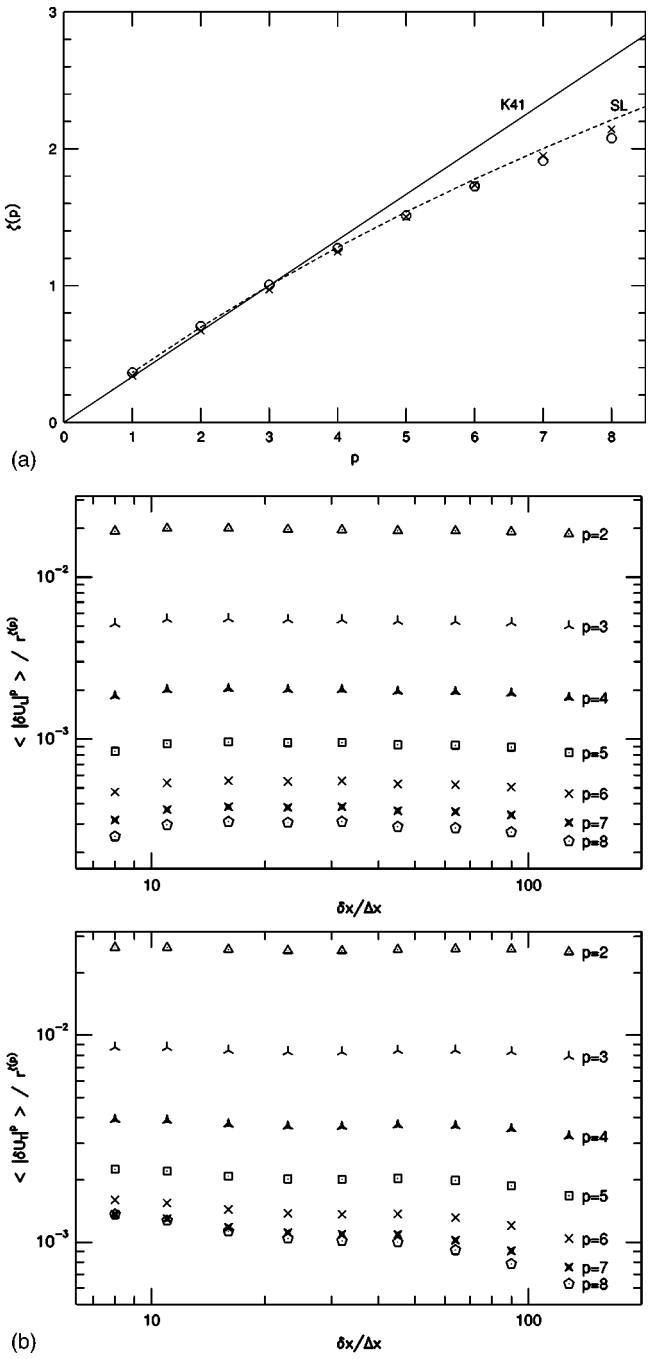

FIG. 8. (a) Scaling exponents $\zeta_p = f(p)$ for run 3 for the longitudinal (cross) and transverse (circles) components of the velocity for the LT method; the solid line represents the K41 law and the dashed line the SL model. (b) Second through eighth order velocity structure functions compensated for by scalings from the She-Leveque (SL) model $[\zeta_p = p/9 + 2 - 2(2/3)^{p/3}]$ for the longitudinal (top) and transverse (bottom) components of the velocity, both using the LT method.

is computed. These local scaling exponents are calculated via a least-squares linear fit in the log-log plane. The significantly larger scatter in the data with the XYZ method [Fig. 6(b)] is primarily due to the larger range of displacements tested with the XYZ method, as compared to the LT method, such displacements extending into the dissipation and energy

containing ranges. However, some of this scatter is attributable to the fact that the XYZ method reinforces the special directions of the driving along the three axes, whereas the LT method avoids this geometrical property of the forcing by angle averaging. Note that there is a slight decrease in scatter as we move towards larger scales. A further indication concerning the errors made in evaluating such scaling exponents is given by dividing the data into a number of different subsets and looking at the variation in the exponents from one set to the other one; for example, in [18], the temporal evolution of such exponents computed on a two turnover time subsampling indicates that the range of variation is limited.

The "4/5" law of Kolmogorov [24] for incompressible flows (see also its extension in [25]) stipulates that $\langle \delta \mathbf{u}_L^3 \rangle = -\frac{4}{5}\epsilon r$ where $\epsilon = -\partial_t \langle \rho_0 u^2 \rangle$ is the kinetic energy transfer rate; it seems to apply as well for the driven supersonic flows we consider in this paper, with $\zeta_3^L \sim 0.99$, although the demonstration of this law relies on relationships stemming from the kinematics of incompressible flows [26]. Note that an independent evaluation of ϵ from the energy input $\langle \mathbf{u} \cdot \mathbf{F} \rangle$ gives $\epsilon \sim 2.3$ whereas the Kolmogorov-like phenomenology gives $\epsilon_K = u_0^3 / l_0 \sim 3.5$, in rough agreement.

Thus the ESS hypothesis [23] can also be applied to supersonic flows; specifically, in order to avoid too noisy a data set, we use rather $S'_{3;L} = \langle |\delta u|_L^3 \rangle$ as the independent variable instead of the distance modulus r. Figure 7(b) displays the data using this methodology, and better scaling is obtained, particularly striking for the longitudinal components [Fig. 7(b), top right]. The range in which a linear fit applies (in these log-log coordinates) with an agreement between both methods is indeed extended, as proposed by the proponents of the ESS method. However, the best estimates of the scaling exponents from the raw data and those given by ESS are essentially the same for this data set. We, therefore, will evaluate exponents with the raw data using scaling of structure functions against distance over ranges of displacements where the two methods agree.

As noted in the different context of magnetohydrodynamic flows [12], other abscissa might be used for the determination of scaling exponents of transverse fields, using the exact scaling law derived in [25] and involving a combination of the transverse and longitudinal components of the velocity. Similarly, a new relationship involving all components of both the velocity and the vorticity in third-order structure functions has been derived in [27] on the basis of the conservation in the inviscid limit of the kinetic helicity $H^V = \langle \mathbf{u} \cdot \omega \rangle$ (see [28] for the derivation of a relation involving correlation functions of the velocity using as well the conservation of kinetic helicity).

Figure 8(a) gives the variations with order p of the scaling exponents of structure functions for run 3 for the velocity using the LT method which has less scatter, as discussed above; a cross (circle) stands for the longitudinal (transverse) components of the velocity field; the solid line represents the K41 law [2], and the dashed line follows the SL model [4] (the log-normal model with its parameter $\mu = 0.21$ is undistinguishable from the SL model at these orders). The longitudinal exponents for this supersonic flow agree, again up to $p = 8$, with those for turbulent incompressible flows and with the SL model. Finally, the longitudinal and transverse exponents differ in what may be an insignificant way, the transverse field being only slightly more intermittent in the sense that its exponents undergo a slightly stronger departure from the K41 linear law. Figure 8(b) shows the velocity structure functions compensated by the scaling expected for the SL model, where $\zeta_p = p/9 + 2 - 2(2/3)^{p/3}$. It can be noted (see Fig. 1 in [18]) that in fact the discrepancy between the ζ_p^L and ζ_p^T exponents stems from the small scales which display more scatter. This result agrees with the finding [8] that the discrepancy between the two sets of exponents diminishes with Reynolds numbers, and vanishes for flows at high Reynolds numbers. A detailed study of the variation of both velocity scaling exponents with time [18] indicates that $\zeta_{p;L} / \zeta_{p;T} > 1$ for all values of p and for all times over a span of $2\tau_{NL}$. The SL model was developed for incompressible fluid turbulence [4]. While the flow discussed here is compressible, we note that the solenoidal component of the flow dominates energetically in this flow. Further, the same kind of filamentary vortex tube structures—pervasive in incompressible flows at high vorticity (see, e.g., [29]) and which are central to the SL model [4]—are numerous as well in our flow [see Fig. 5(b)].

B. Intermittency of the density and entropy

Compressible flows generally have two independent thermodynamic fields. Density and entropy are examined here because density is a fundamental conserved quantity of the flow, and entropy is a constant of the flow except for source terms such as dissipation and the σT^4 cooling term used in our driven flows. In the low to moderate Mach number flows considered here, advective terms appear to dominate over these source terms. Hence, the entropy tends to behave like a passively advected scalar, for which there is a predicted scaling of the structure functions which comes from studies of incompressible flow [9].

One can compute the intermittency exponents of the entropy and of the logarithm of the density in a manner similar to that used with the velocity field. For the polytropic ideal gas considered here the entropy can be written as $\mathcal{S} = S_0 + S_1 \ln[(p/p_0)/(\rho/\rho_0)^\gamma]$, where p_0 and ρ_0 are the average pressure and density and S_i are constants related to both physical units and gas constants (such as molecular weight). For given pressure and density fields, the scaling of the structure functions of entropy is independent of the constants S_i, p_0, and ρ_0. The data is given in Fig. 9, with triangles for the entropy and squares for the logarithm of the density. The entropy appears significantly more intermittent than the velocity, in a manner somewhat reminiscent of the passive scalar. Contrary to the case of the velocity, the exponents decrease at high p. Note that the assertion stipulating that the ζ_p curve for a given variable is convex relies on the assumption of the existence of a bound for that field; such a bound may not exist for the log of density nor the entropy, since, e.g., rarefaction waves can lead to an arbitrarily large density contrast ρ_{max} / ρ_{min}, and spatial variations in the dissipation may lead to arbitrarily large entropy jumps.

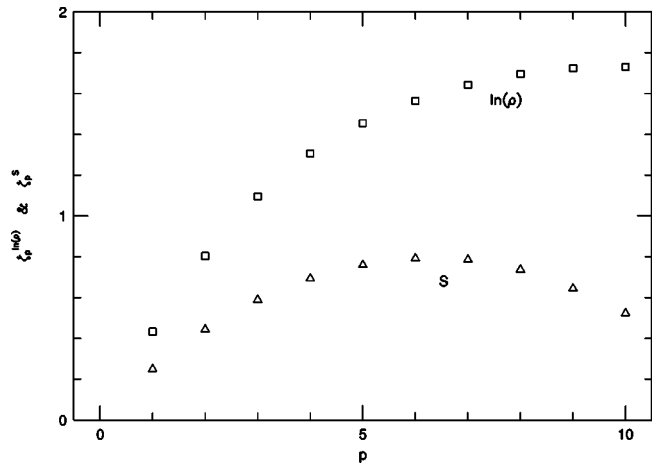

FIG. 9. Scaling exponents $\zeta_p = f(p)$ for the logarithm of the density (squares), and for the entropy (triangles).

C. The effect of anisotropy: Driving with a one-dimensional shear wave

In the case of run 1 with a one-dimensional shear wave driving in the X direction and varying in the Z direction, the resulting flow displays clear signs of anisotropy, as can be observed in Fig. 10: whereas the two directions orthogonal to the driving are in equipartition, there is an excess of energy in the X component of the velocity by a factor of 100 at $k = k_{min}$; it decreases to a factor of about 3 at $k = 3k_{min}$, and continues to decrease with k until all three components of the velocity are in equipartition at $k = 20k_{min}$, thus recovering some isotropy in the small scales at the level of second-order correlations. The Kolmogorov law is better achieved for the unidirectional spectrum with the highest energy level, as seen, e.g., in the power spectrum of u_x. Similarly, this anisotropy is noticeable insofar as the scaling exponents of the velocity structure functions at all orders in the X direction differ substantially from the other two directions, as can be seen from Fig. 11 giving the $\zeta_p^{L,T}$ exponents as a function of order p for all nine components of the matrix that can be constructed with the three components of the velocity and

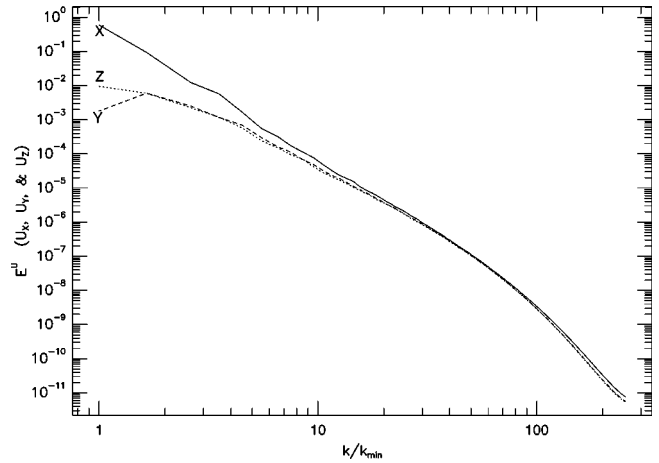

FIG. 10. Energy spectra for run 1 in the direction of the driving (solid line), and in the Y (dashed line) and Z (dotted line) directions.

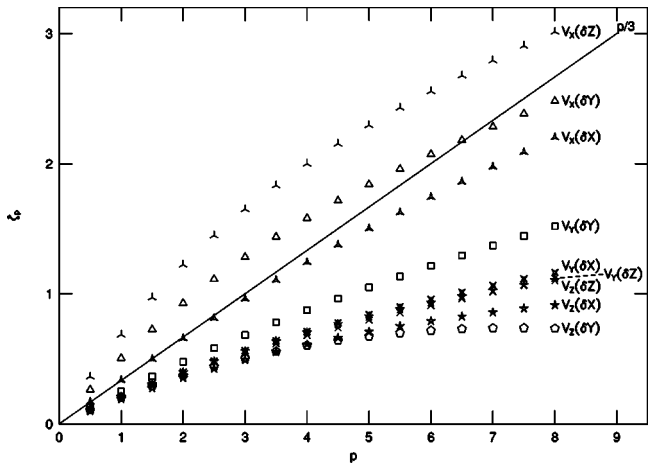

FIG. 11. Scaling exponents of the longitudinal and transverse velocity for run 1 for all three directions (see labels). Only the X component of velocity is directly driven; the driving acceleration varies as a sine wave in the Z direction.

taking the displacements in either of the three directions (see labels); no averaging over multiple directions is performed here in contrast to run 3, a three-way driven flow. The average is done on six temporal snapshots spanning two eddy turnover times, and with the scaling applied in the inertial interval $[32\delta x,\ 64\delta x]$. Each of the coordinate directions is special: the driving force is applied only to u_x and the driving force varies only in Z. It is notable that of the nine anomalous exponents shown, the ones involving δu_x (i.e., the directly driven velocity component) have the largest values, and that, of these three, δu_x varying in the Z direction (the direction the driving varies in) is the largest. The scatter in ζ_p for $p > 6$ may be due to insufficient statistics, the six snapshots of this 512^3 data providing about 8×10^8 points. However, the scatter in ζ_2 and ζ_3 is undoubtedly due to the anisotropy of the driving force, which is evidently felt at scales an order of magnitude smaller than the scale of the driving.

IV. THE ENERGY TRANSFER

We now examine the scaling behavior of the moments of the energy transfer

$$\langle |\epsilon(\mathbf{r})|^p \rangle \sim r^{\tau_p}.$$

The computation of the energy transfer averaged over a ball of linear dimension r is performed using a Gaussian filter, the Fourier width of the filter K_F being taken as representative of the given scale, $r \sim K_F^{-1}$. Here, ϵ is based on the contribution to the evolution of the kinetic energy of the flow on resolved scales due to the effect of the subfilter-scale stresses through the nonlinear term of the Navier-Stokes equations. The equations of motion are Favre filtered. From the filtered continuity and momentum equations the equation of evolution for the kinetic energy of the resolve fields is derived. Specifically, we use a Gaussian Favre filter

$$\tilde{Q}=\overline{\rho Q}/\overline{\rho}, \quad \overline{Q}(x)=\frac{1}{N}\int e^{-[K_F(x-x_1)]^2/2}Q(x_1)d^3x_1, \tag{8}$$

$$N=\int e^{-(K_F x)^2}d^3x \tag{9}$$

for these compressible flows.

The momentum equation for the filtered velocity is

$$\frac{\partial\overline{\rho}\tilde{U}}{\partial t}+\partial_j(\overline{\rho}\tilde{U}_i\tilde{U}_j)=\partial_i p+\partial_j\tau_{ij}, \tag{10}$$

and the subfilter-scale stress is

$$\tau_{ij}=\overline{\rho U_i U_j}-\overline{\rho}\tilde{U}_i\tilde{U}_j. \tag{11}$$

The kinetic energy in the resolved (filtered) fields

$$\tilde{K}=\frac{1}{2}\overline{\rho}\tilde{U}^2 \tag{12}$$

evolves according to

$$\frac{\partial\tilde{K}}{\partial t}=\cdots+\tilde{U}_i\partial_j\tau_{ij}=\cdots+\partial_j(\tilde{U}_i\tau_{ij})-(\partial_j\tilde{U}_i)\tau_{ij}. \tag{13}$$

While $\tilde{U}_i\partial_j\tau_{ij}$ is not Galilean invariant, the term $(\partial_j\tilde{U}_i)\tau_{ij}$ is invariant under a velocity boost. The term $\partial_j(\tilde{U}_i\tau_{ij})$ is the effect on $\tilde{K}$ of the kinetic energy flux $(\tilde{U}_i\tau_{ij})$ due to the SGS stresses: it only transports the kinetic energy of the resolved scale flow, and does not correspond to any forward or back transfer of energy from resolved to unresolved fields. Hence, we identify

$$\epsilon(\mathbf{r})=-(\partial_j\tilde{U}_i)\tau_{ij} \tag{14}$$

as the local SGS energy flux due to the nonlinear terms of the momentum equations. The analysis is performed on two snapshots at $t=3$ and $t=9.2$, with nearly identical scalings: the values of τ_1, τ_2, and τ_3 each differ by about 10% between the two times. Given the nonambiguous scaling observed for this data in Fig. 12, we feel there is no need, given the high cost of this specific computation, to go over the whole temporal data set.

For the fourfold range of scales considered in Fig. 12 (top), within the inertial range, the scatter is small with a maximum deviation $\sim 1.5\%$; the scaling for $p=1/3$, 1, and 3 is given in Fig. 12 (bottom). Note that $|\epsilon_r|\sim$ constant in that range. We also performed a check of the refined similarity hypothesis of Kolmogorov (KRSH) which stipulates that $\zeta_p=p/3+\tau_{p/3}$; this relationship stems from evaluating the local energy transfer ϵ_l at scale l as $\epsilon_l\sim u_l^3/l$; τ_p is shown with triangles, whereas the cross (circle) gives $\zeta_{3p}-p$ for the longitudinal (transverse) components of the velocity; finally, the solid line is for K41, the dotted line for the She-Leveque model, and the dashed line for the log-normal model with $\mu=0.21$ (see also [30]). Figure 7(b) shows the spread in our measure of ζ_8 to be roughly ± 0.1 for the longitudinal velocity and about ± 0.2 for the transverse velocity. Hence, our data, overall, is consistent with the Kolmogorov KRSH hypothesis within the error bars of our measures of ζ_p, despite the fact that this is a supersonic flow and exchanges with the pressure field constitute about 10% of the total energy transfer. The same conclusion concerning the validity of the KRSH hypothesis is reached in [8] for incompressible fluids.

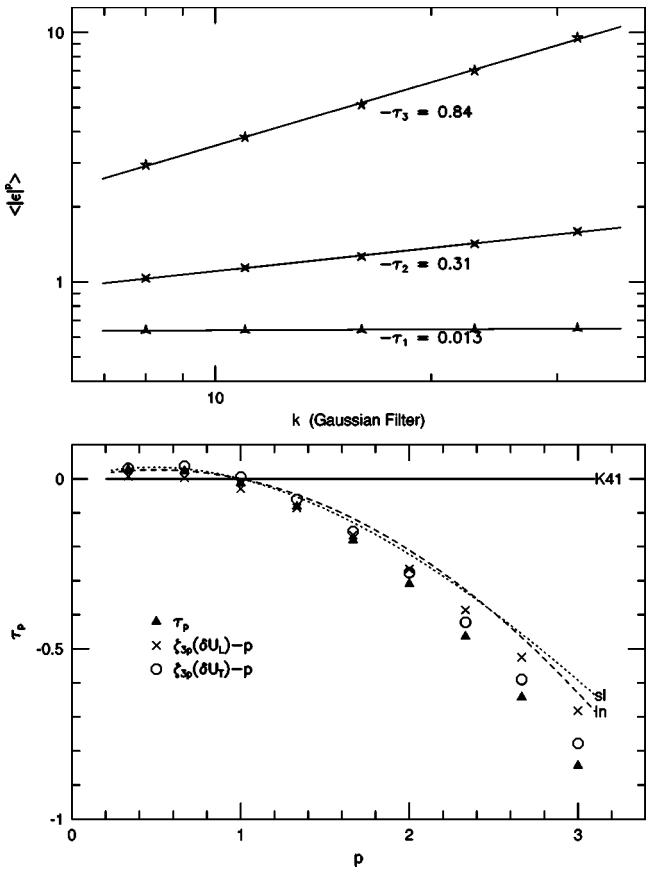

FIG. 12. Top: variation with the Fourier width of the filter of the first three moments of the local energy transfer ($p=1$, 2, and 3) at time $t=9.2$. Bottom: scaling exponents of the transfer together with a test of the Kolmogorov refined similarity hypothesis; the log-normal model with $\mu=0.21$ (label ln) and the She-Leveque (label sl) models are also shown.

V. CONCLUSION

For the sustained supersonic flows examined in this paper, the intermittency exponents for the velocity field are similar to those for the incompressible case although numerous shocks are present at all times [31]: these Mach one flows, with $\chi=E^C/E^V\sim 0.03$—measuring the relative shock-to-vortex energy—have incompressible-like behavior as far as the scaling of structure functions is concerned.

In that light, it should be remembered that observations for both the solar wind and the interstellar medium give indications that the behavior in such turbulent compressible media is interpretable in terms of classical turbulence, displaying histograms with strong non-Gaussian wings, and with—at least in one case—$\langle\delta\mathbf{u}^3\rangle\sim r$ [11]. This raises the

question of the universality of the Kolmogorov phenomenology, beyond its original domain of applicability. For example, it is not clear whether the inclusion of a magnetic field breaks such a universality because of the interactions of turbulent eddies with Alfvén waves propagating along the lines of a strong background magnetic field, and leading to substantially lesser energy transfer to small scales as embodied in the Iroshnikov-Kraichnan (''IK'') phenomenology developed in [32]. Whether it is the K41 or the IK phenomenology that applies to such flows—i.e., whether in the former case local interactions (between modes of comparable wavelengths) dominate the nonlinear transfer, or in the latter nonlocal Alfvénic anisotropic transfer is dominant—is still an open question presently (see, e.g., [33]).

In order to ascertain more precisely the characteristics of the compressible component of supersonic flows besides the information already given here on the density and entropy, one could examine as well the pressure and temperature scaling laws; the former will allow for another comparison with the incompressible case by looking, e.g., at histograms, and the latter is of particular interest to the astrophysical community since it relates more directly to observations. Another piece of information will come from an evaluation of the scaling exponents of the compressible part of the velocity u_C, using the standard Helmholtz decomposition. Will it follow, at all orders, the incompressible component of the velocity, which energetically is prevalent? We already know that for $p=2$, the spectrum of the compressible part of the velocity follows a Kolmogorov law (with possible intermittency corrections), as opposed to the classical k^{-2} law as in the shock spectrum of the Burgers equation. This can be interpreted in terms of the Lundgren model of a spiral vortex [34] (see also [35]) entraining the medium surrounding it: the curvature in the velocity field that develops, through the Biot-Savart law, in the vicinity of a strong vortex tube, also imprints on the divergence of the velocity; this may be sufficient to bring about a $-5/3$ scaling [36]. Do higher orders of the structure functions of the longitudinal velocity field follow the scaling of the solenoidal component for this run with $\chi \sim 0.03$? Furthermore, what will be the scaling laws for compressible flows with a drastically different value in the steady state of χ, as could be obtained with a mostly compressible forcing? Indeed, another physical problem worth examining is the one dominated energetically by shocks, a regime which may arise through a driving in the heat equation, as that stemming from either cosmic rays or ionization winds or a blast wave emanating from a supernova in the interstellar medium (ISM). Will such flows behave again *à la* Kolmogorov, or rather as for the Burgers equation with its *N*-wave system? The production of vorticity may be essential in this case; with either rotation (of strength Ω_0) or magnetic fields (of strength B_0) present in the ISM, vorticity will be produced; but with both Ω_0 and B_0 equal to zero, the outcome may be different. In view of the huge observational effort made presently in the community studying the ISM, and giving already access to low-order structure functions of the velocity, these questions merit attention and are left for future work.

ACKNOWLEDGMENTS

This work was supported at the University of Minnesota by the Department of Energy, through Grant Nos. DE-FG02-87ER25035 and DE-FG02-94ER25207, contracts from Livermore and Los Alamos; by the National Science Foundation, through its PACI program at NCSA, through a research infrastructure grant, CDA-950297, and also through a Grand Challenge Application Group award ASC-9217394, through a subcontract from the University of Colorado; and from NASA, through a Grand Challenge team award, NCCS-5-151, through a subcontract from the University of Chicago. We would also like to acknowledge local support from the University of Minnesota's Minnesota Supercomputing Institute. This work was supported in Nice by a CNRS PN–PCMI grant. All are gratefully acknowledged.

[1] D. Porter, P. Woodward, and A. Pouquet, Phys. Fluids **10**, 237 (1998).
[2] A. Kolmogorov, Dokl. Akad. Nauk SSSR **31**, 538 (1941).
[3] U. Frisch, *Turbulence: The Legacy of Kolmogorov* (Cambridge University Press, Cambridge, England, 1995).
[4] Z. S. She and E. Lévêque, Phys. Rev. Lett. **72**, 336 (1994).
[5] B. Dubrulle, Phys. Rev. Lett. **73**, 959 (1994).
[6] H. Politano and A. Pouquet, Phys. Rev. E **52**, 636 (1995).
[7] J. Herwiejer and W. Van DeWater, in *Advances in Turbulence VI*, edited by V. R. Benzi (Kluwer, Dordrecht, 1995), pp. 210–216; O. Boratav, Phys. Rev. E **56**, R2363 (1997); A. Noullez, G. Wallace, W. Lempert, R. B. Miles, and U. Frisch, J. Fluid Mech. **339**, 287 (1997).
[8] S. Chen, K. Sreenivasan, M. Nelkin, and N. Cao, Phys. Rev. Lett. **79**, 1253 (1997); R. Antonia and T. Zhou, in *Advances in Turbulence VII*, edited by U. Frisch (Kluwer, Dordrecht, 1998), pp. 227–230.
[9] Z. Warhaft, Annu. Rev. Fluid Mech. **32**, 203 (2000).
[10] L. Burlaga, J. Geophys. Res. **96**, 5847 (1991); M. Tu and E. Marsch, Space Sci. Rev. **73**, 1 (1995).
[11] E. Falgarone, in *Interstellar Turbulence*, edited by J. Franco and A. Carraminama (Cambridge University Press, Cambridge, England, 1999); G. Joncas, *ibid.*
[12] For magnetized but incompressible flows, see H. Politano and A. Pouquet, Phys. Rev. E **57**, R21 (1998); J. Geophys. Lett. **25**, 273 (1998); H. Politano, A. Pouquet, and V. Carbone, Europhys. Lett. **43**, 516 (1998); T. Gomez, H. Politano, and A. Pouquet, Phys. Fluids **11**, 2298 (1999).
[13] P. Woodward and P. Colella, J. Comput. Phys. **54**, 115 (1984).
[14] D. Porter, A. Pouquet, and P. R. Woodward, Theor. Comput. Fluid Dyn. **4**, 13 (1992).
[15] I. V. Sytine, D. Porter, P. Woodward, S. Hodson, and K-H. Winkler, J. Comput. Phys. **158**, 225 (2000).
[16] D. Porter, A. Pouquet, and P. R. Woodward, Lect. Notes Phys. **462**, 51 (1995).
[17] D. Porter, A. Pouquet, I. Sytine, and P. Woodward, Physica A **263**, 263 (1999).

[18] D. Porter, A. Pouquet, and P. R. Woodward, in *Advances in Turbulence VII*, edited by U. Frisch (Kluwer, Dordrecht, 1998), pp. 255-258.
[19] T. Passot and A. Pouquet, J. Fluid Mech. **181**, 441 (1987).
[20] I. Arad, L. Biferale, I. Mazzitelli, and F. Toschi, Phys. Rev. Lett. **82**, 5040 (1999).
[21] D. Porter, A. Pouquet, and P. R. Woodward, Phys. Rev. Lett. **68**, 3156 (1992).
[22] E. Vázquez-Semadeni, T. Passot, and A. Pouquet, Astrophys. J. **473**, 881 (1998).
[23] R. Benzi, S. Ciliberto, R. Tripiccione, C. Baudet, F. Massaioli, and S. Succi, Phys. Rev. E **48**, R29 (1993).
[24] A. Kolmogorov, Dokl. Akad. Nauk SSSR **32**, 16 (1941).
[25] R. Antonia, M. Ould-Rouis, F. Anselmet, and Y. Zhu, J. Fluid Mech. **332**, 395 (1997); the equivalent law for the passive scalar is derived in A. M. Yaglom, Dokl. Akad. Nauk SSSR **69**, 743 (1949) [see also L. Fulachier and R. Dumas, J. Fluid Mech. **77**, 257 (1976)].
[26] The same type of linear scaling holds as well for the Burgers equation with $\langle \delta u^3(r) \rangle = -12\epsilon r$.
[27] T. Gomez, H. Politano, and A. Pouquet, Phys. Rev. E **61**, 5321 (2000).
[28] O. Chkhetiani, JETP Lett. **10**, 808 (1996).
[29] A. Vincent and M. Meneguzzi, J. Fluid Mech. **258**, 245 (1994).
[30] O. Boratav, Phys. Fluids **10**, 2122 (1998).
[31] In a flow with a rms Mach number of unity, the actual strength of a shock is given either by its pressure jump, or by its velocity relative to the upstream one. The latter can be approximated by the velocity differences Δu over distances Δx; an examination of these histograms reveals that $\Delta u/c_s \sim 1$ for $\Delta x/\delta x = 16$ over roughly 10^4 points for each snapshot.
[32] P. Iroshnikov, Sov. Astron. **7**, 566 (1963); R. H. Kraichnan, Phys. Fluids **8**, 1385 (1965).
[33] A. Pouquet, in *Interstellar Turbulence*, Proceedings of the 2nd Guillermo Haro Conference, edited by J. Franco and A. Carraminana (Cambridge University Press, Cambridge, 1999), pp. 87–94.
[34] T. Lundgren, Phys. Fluids **25**, 2193 (1982).
[35] A. Gilbert, Phys. Fluids A **5**, 2831 (1993).
[36] T. Gomez, thèse, Université Paris VI, 1999; T. Gomez, H. Politano, M. Larchevêque, and A. Pouquet, Phys. Fluids **13**, 2065 (2001).